Applied Mathematical Modelling 48 (2017) 196–207

Contents lists available at ScienceDirect

Applied Mathematical Modelling

journal homepage: www.elsevier.com/locate/apm

Electro-mechanical shear buckling of piezoelectric nanoplate using modified couple stress theory based on simplified first order shear deformation theory

Mohammad Malikan

Department of Mechanical Engineering, Islamic Azad University, Mashhad, Iran

ARTICLE INFO

Article history:
Received 6 December 2016
Revised 6 March 2017
Accepted 28 March 2017
Available online 5 April 2017

Keywords:
Electro-mechanical shear buckling
Piezoelectric nanoplate
Modified couple stress theory
Simplified first order shear deformation theory

ABSTRACT

This paper studies the electro-mechanical shear buckling analysis of piezoelectric nanoplate using modified couple stress theory with various boundary conditions.In order to be taken electric effects into account, an external electric voltage is applied on the piezoelectric nanoplate. The simplified first order shear deformation theory (S-FSDT) has been employed and the governing differential equations have been obtained using Hamilton's principle and nonlinear strains of Von-Karman. The modified couple stress theory has been applied to considering small scale effects. An analytical approach was developing to obtain exact results with various boundary conditions. After all, results have been presented by change in some parameters, such as; aspect ratio, effect of various boundary conditions, electric voltage and length scale parameter influences. At the end, results showed that the effect of external electric voltage on the critical shear load occurring on the piezoelectric nanoplate is insignificant.

1. Introduction

Piezoelectric materials represent a particularly interesting class of smart materials, possessing highly efficient electromechanical coupling, i.e., piezoelectricity, which is a unique feature for non-centrosymmetric dielectric materials [1]. With the development of nanotechnology and synthesis techniques, a variety of piezoelectric nanomaterials have been synthesized under different growth conditions. In general, nanostructured materials are defined as materials with morphological features on the nano-scale, which are smaller than one tenth of a micrometer in at least one direction [2].

Such nanostructured materials may possess special physical and mechanical properties stemming from their nano-scale features. In particular, the enhanced electromechanical coupling of piezoelectric nanomaterials makes them attractive for the potential applications as generators, sensors and transducers [3–5], in nanoelectromechanical systems (NEMS). In order to further explore the piezoelectric nanomaterials and apply them commercially, it is of great importance to get a thorough and comprehensive understanding of their electromechanical coupling properties at the nano-scale.

Over the past decade, many researches have been being examined in order to study the stability behavior of nano structures [6–36]. Malekzadeh et al. [8] considered the small scale effect on the thermal buckling of orthotropic arbitrary straight-sided quadrilateral nanoplates embedded in an elastic medium via classical plate theory. Ke et al. investigated the nonlinear vibration [9] and post-buckling [10] behaviors of nonlocal Timoshenko piezoelectric nanobeams under combined thermo-electro-mechanical loadings. Murmu et al. [11] conducted buckling analysis of bi-layer nano graphene in nonlocal theory

E-mail addresses: mohammad.malikan@yahoo.com, malikan.mohammad@gmail.com

http://dx.doi.org/10.1016/j.apm.2017.03.065
0307-904X/

under biaxial compression via analytical solution using the classical plate theory with linear strains. It also demonstrated that nonlocal critical load was always less than local. Malekzadeh and Alibeygi [12] analyzed the thermal buckling of orthotropic single layer graphene sheet using nonlinear elastic foundation. The classical theory and differential quadrature method were used, together with the Winkler elastic foundation which was modeled with the nonlinear spring. Mohammadi et al. [13] studied the shear buckling of orthotropic rectangular single layer nanoplate in thermal environment by classical plate theory. They showed that the difference between the shear buckling load calculated by isotropic and orthotropic plates decreases with increasing nonlocal parameter. Radic et al. [14] published a study on mechanical buckling of multi-layers rectangular graphene sheet based on an elastic foundation and found that the nonlocal effect had great influence on higher buckling modes. The exact solution for vibrations and biaxial buckling of multilayers graphene sheet based on the Winkler elastic foundation were investigated by Murmu and co-workers [15]. The presented equations utilized classical plate theory and proved that the critical temperature and natural frequencies were further affected by reducing the Winkler coefficient in high modes. Anjomshoa et al. [16] derived mechanical buckling equations of multi-layers of rectangular graphene sheet placed on an elastic foundation using the classical plate theory and finite element numerical method. Radebe and Adali [17] studied the buckling of rectangular nano-plates with uncertain orthotropic material properties using non-local theory. They considered nano-plate as a non-local plate to take the small-size effects into account with small-scale parameter also taken to be uncertain. They studied the effect of small scale on natural frequencies. Vibration and buckling analysis of a piezoelectric nanoplate considering surface effects and in-plane constraints have been presented by Jiang and Yan [18]. Golmakani and Rezatalab [19] conducted a study on the biaxial buckling of single layer graphene plate by considering the elastic foundation and nonuniform mechanical load. The results showed that by neglecting the elastic foundation, when the small scale effects are reduced, the critical load also has decreased. Challamel et al. [20] proposed the buckling and vibrations of micro structured rectangular plates considering phenomenological and lattice-based nonlocal continuum models. Radic and Jeremic [21] studied the thermal buckling of double-layered graphene sheets embedded in an elastic medium with various boundary conditions using a nonlocal new first-order shear deformation theory. Their results showed that in nonlinear distributions of temperature all over the thickness of plate, have a higher value of critical buckling temperatures for lower values of aspect ratio. Malikan et al. [22] recently published buckling of double-layered nanoplate under shear and thermal loads based on the elastic matrix using differential quadrature method. They showed that, the effect of type of shear loading on the nonlocal results is more than local results. Also, in thermal buckling analysis, the most important results being that whether the boundary conditions have more flexibility, by increasing the dimension's ratio, the results of critical temperature were tightly close together in nonlocal and local analysis.

This paper investigates novel theoretical formulation on piezoelectric nanoplates. Regarding the FSDT, we could not get the right value for shear correction factor to consider the shear stress distribution in thickness direction. Therefore, the simplified first order shear deformation theory (S-FSDT) that provides a welcome alternative to solve the problem has been investigated. Afterward, the nonlinear strain of Von-Karman has been considered. In addition, in order to study the length scale, because of the fact that there is a difficulty with Eringen nonlocal theory to consider nano materials behavior while it is applying on the nonlocal stress resultants in deriving of governing equations, because of the presence of variable nonlocal parameter. So, the modified couple stress theory has been employed in the research. Furthermore, the exact solution is used to solve the stability equations in various boundary conditions as well as free edges. Consequently, the effects of different parameters such as; changes in the length scale parameter, external electric voltage, aspect ratio and boundary effects of edges in various conditions under in-plane shear load have been demonstrated.

2. Formulation

A rectangular piezoelectric nanoplate is considered with thickness h, the length L_x, and the width L_y as shown in Fig. 1. Of the many shear deformable plate theories proposed over the years, the FSDT is fundamentally simpler to adopt for modeling of the shear deformation behavior of plates. FSDT, are widely in use, even today, because of its simplicity. It is now well-known that in plate analysis, shear deformation effects become important not only for thick plates but even for thin plates [23]. As classical plate theory (CPT) does not take into account shear effects, many theories got evolved to address the deficiency. According to the FSDT, the following displacement field can be expressed as:

$$U(x,y,z) = u(x,y) + z\varphi(x,y), \tag{1a}$$

$$V(x,y,z) = v(x,y) + z\psi(x,y), \tag{1b}$$

$$W(x,y,z) = w(x,y), \tag{1c}$$

where u, v and w are the displacement components along x, y and z directions, respectively. Moreover, ϕ and ψ are the rotational displacement about the y and x directions, respectively. In this theory, the shear stress in thickness direction is constant value which in fact is not true. But, in the S-FSDT theory, it is assumed that the transverse displacement (w) is divided into the bending component (w_b) and the shear component (w_s) which means that [24]:

$$w = w(bending) + w(shear). \tag{2}$$

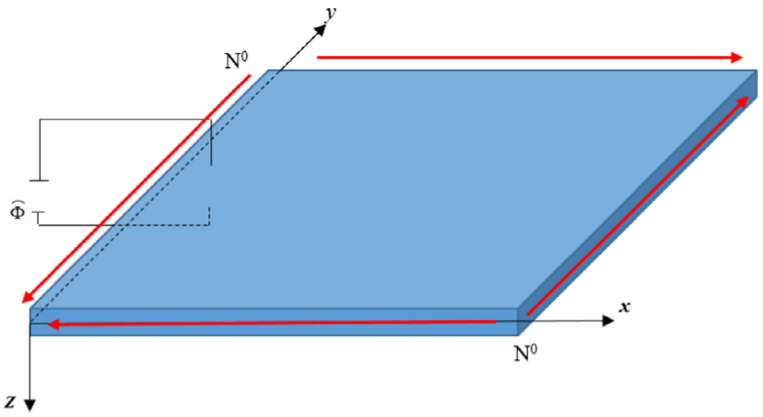

Fig. 1. Schematic diagram of rectangular piezoelectric nanoplate.

Also, the rotation variable in the S-FSDT is expressed in terms of the bending component only:

$$\varphi = -\frac{\partial w_b}{\partial x}$$
$$\psi = -\frac{\partial w_b}{\partial y}. \tag{3}$$

With implementation Eqs. (2) and (3) into Eq. (1) the S-FSDT displacement field can be written as follows:

$$\begin{cases} U(x\ ,\ y\ ,\ z) = u(x,y) - z\dfrac{\partial w_b}{\partial x} \\ V(x\ ,\ y\ ,\ z) = v(x,y) - z\dfrac{\partial w_b}{\partial y} \\ W(x,y,z) = w_b(x,y) + w_s(x,y) \end{cases}. \tag{4}$$

In recent years, various size dependent continuum theories such as couple stress theory, modified couple stress theory, strain gradient theory and nonlocal elasticity theory have proposed. These theories are comprised of information about the inter-atomic forces and internal lengths. Among these theories, nonlocal elasticity theory of Eringen has been widely applied. But in the theory, we cannot find unique result, since we have to use the variable nonlocal parameter. The classical couple stress theory is one of the higher order continuum theories, which contains two additional material length scale parameters besides the classical constants for an elastic material, elaborated by Mindlin and Tieresten [25], Toupin [26], and Koiter [27]. In fact, couple stress theory is a special case of Micropolar theory proposed by Cosserat brothers [28]. Newly, a modified couple stress theory, which contains only one additional material length scale parameter in addition to the classical material constants, was proposed by Yang et al. [29]. The modified couple stress theory is more useful than classical one due to symmetric couple stress tensor. According to this higher-order continuum theory and using the Hamilton's principle, the governing equations as well as the related boundary conditions along the edges of rectangular piezoelectric nanoplate can be derived. The equation of the total potential energy (V) is expressed as:

$$V = U + \Omega. \tag{5}$$

Here U is strain energy and Ω is work done by external loads. The virtual strain energy can be calculated as:

$$\delta U = \iiint_{v} \left(\sigma_{ij}\delta\varepsilon_{ij} + m_{ij}\delta\chi_{ij} + D_k E_k\right) dV = 0, \tag{6}$$

where σ_{ij}, ε_{ij}, m_{ij}, χ_{ij}, D_k, E_k, are stress tensor, strain tensor, deviatoric part of the couple stress tensor, symmetric curvature tensor, electric displacement and electric field, respectively [30–32].

$$\sigma_{ij} = C_{ijkl}\varepsilon_{kl} - e_{kij}E_k, \quad D_i = e_{ikl}\varepsilon_{kl} + \kappa_{kij}E_k, \tag{7}$$

$$m_{ij} = 2G_{xy}l^2\chi_{ij}, \varepsilon_{ij} = \frac{1}{2}\left(\frac{\partial u_i}{\partial x_j} + \frac{\partial u_j}{\partial x_i} + \frac{\partial u_k}{\partial x_i}\frac{\partial u_k}{\partial x_j}\right), \quad i,j = 1,2;\ k = 3 \tag{8}$$

$$\chi_{ij} = \frac{1}{2}\left(\frac{\partial \theta_i}{\partial x_j} + \frac{\partial \theta_j}{\partial x_i}\right), \quad \mathrm{i,j} = 1,2,3; \quad \theta_i = \frac{1}{2}\lambda_{ijk}\mathrm{U}_{k,j}, \tag{9}$$

where l is a material length scale parameter that is related to size effect, and θ is the rotation vector. Also, C_{ijkl}, e_{kij},κ_{kij} are elastic constant, piezoelectric constant and dielectric constant, respectively. The tensors associated in the displacement field

in Eqs. (7–9) are:

$$\begin{cases} \varepsilon_{xx} = \dfrac{\partial u}{\partial x} - z\dfrac{\partial^2 w_b}{\partial x^2} + \dfrac{1}{2}\left(\dfrac{\partial w_b}{\partial x}\right)^2 + \dfrac{1}{2}\left(\dfrac{\partial w_s}{\partial x}\right)^2 + \dfrac{\partial w_b}{\partial x}\dfrac{\partial w_s}{\partial x} \\ \varepsilon_{yy} = \dfrac{\partial v}{\partial y} - z\dfrac{\partial^2 w_b}{\partial y^2} + \dfrac{1}{2}\left(\dfrac{\partial w_b}{\partial y}\right)^2 + \dfrac{1}{2}\left(\dfrac{\partial w_s}{\partial y}\right)^2 + \dfrac{\partial w_b}{\partial y}\dfrac{\partial w_s}{\partial y} \\ \gamma_{yz} = \dfrac{\partial w_s}{\partial y} \\ \gamma_{xz} = \dfrac{\partial w_s}{\partial x} \\ \gamma_{xy} = \left(\dfrac{\partial u}{\partial y} + \dfrac{\partial v}{\partial x}\right) - 2z\dfrac{\partial^2 w_b}{\partial x \partial y} + \left(\dfrac{\partial w_b}{\partial x} + \dfrac{\partial w_s}{\partial x}\right)\left(\dfrac{\partial w_b}{\partial y} + \dfrac{\partial w_s}{\partial y}\right) \end{cases}, \tag{10a-e}$$

$$\begin{cases} \theta_1 = \dfrac{1}{2}\left(2\dfrac{\partial w_b}{\partial y} + \dfrac{\partial w_s}{\partial y}\right) \\ \theta_2 = -\dfrac{1}{2}\left(2\dfrac{\partial w_b}{\partial x} + \dfrac{\partial w_s}{\partial x}\right) \\ \theta_3 = \dfrac{1}{2}\left(\dfrac{\partial v}{\partial x} - \dfrac{\partial u}{\partial y}\right) \end{cases}, \tag{11a-c}$$

$$\begin{cases} \chi_x = \dfrac{1}{2}\left(2\dfrac{\partial^2 w_b}{\partial x \partial y} + \dfrac{\partial^2 w_s}{\partial x \partial y}\right) \\ \chi_y = \dfrac{1}{2}\left(-2\dfrac{\partial^2 w_b}{\partial x \partial y} - \dfrac{\partial^2 w_s}{\partial x \partial y}\right) \\ \chi_{xy} = \dfrac{1}{4}\left(-2\dfrac{\partial^2 w_b}{\partial x^2} + 2\dfrac{\partial^2 w_b}{\partial y^2} - \dfrac{\partial^2 w_s}{\partial x^2} + \dfrac{\partial^2 w_s}{\partial y^2}\right) \\ \chi_{xz} = \dfrac{1}{4}\left(\dfrac{\partial^2 v}{\partial x^2} - \dfrac{\partial^2 u}{\partial x \partial y}\right) \\ \chi_{yz} = \dfrac{1}{4}\left(-\dfrac{\partial^2 u}{\partial y^2} + \dfrac{\partial^2 v}{\partial x \partial y}\right) \end{cases}, \tag{12a-e}$$

$$e_{kij} = \begin{bmatrix} 0 & 0 & \widehat{e}_{31} \\ 0 & 0 & \widehat{e}_{31} \\ \widehat{e}_{15} & 0 & 0 \\ 0 & \widehat{e}_{15} & 0 \\ 0 & 0 & 0 \end{bmatrix}, \quad \kappa_{kij} = \begin{bmatrix} \widehat{\kappa}_{11} & 0 & 0 \\ 0 & \widehat{\kappa}_{11} & 0 \\ 0 & 0 & \widehat{\kappa}_{33} \end{bmatrix}, \quad E_k = \begin{Bmatrix} \widehat{E}_x \\ \widehat{E}_y \\ \widehat{E}_z \end{Bmatrix}. \tag{13a-c}$$

To confirm the Maxwell equation, the distribution of external electric potential for the present nanoplate model is assumed as a combination of a cosine and linear variation [32–34].

$$\widehat{\Phi}(x, y, z) = -\cos(\beta z)\Phi(x, y) + \frac{2zV_0}{h}, \tag{14}$$

where $\beta = \pi/h$; $\Phi(x, y)$ is the spatial and time vibration of the electric potential in the mid-plane of the nanoplate, and V_0 is the external electric voltage. Then, the components of electric field can be written as:

$$E_k = \begin{Bmatrix} -\dfrac{\partial \widehat{\Phi}}{\partial x} \\ -\dfrac{\partial \widehat{\Phi}}{\partial y} \\ -\dfrac{\partial \widehat{\Phi}}{\partial z} \end{Bmatrix} = \begin{Bmatrix} \cos(\beta z)\dfrac{\partial \Phi}{\partial x} \\ \cos(\beta z)\dfrac{\partial \Phi}{\partial y} \\ -\beta \sin(\beta z)\Phi - \dfrac{2V_0}{h} \end{Bmatrix}. \tag{15a-c}$$

Using the principle of minimum total energy ($\delta_V = 0$) the nonlinear constitutive equations are derived as:

$$\delta U = 0; N_{x,x} + N_{xy,y} + 1/4Y_{xz,xy} + 1/4Y_{yz,yy} = 0, \tag{16a}$$

$$\delta V = 0; N_{xy,x} + N_{y,y} - 1/4Y_{xz,xx} - 1/4Y_{yz,xy} = 0, \tag{16b}$$

$$\delta W_b = 0; Q_{x,x} + Q_{y,y} + N_{xx}\left(\frac{\partial^2 w_s}{\partial x^2} + \frac{\partial^2 w_b}{\partial x^2}\right) + N_{yy}\left(\frac{\partial^2 w_s}{\partial y^2} + \frac{\partial^2 w_b}{\partial y^2}\right) + 2N_{xy}\left(\frac{\partial^2 w_b}{\partial x \partial y} + \frac{\partial^2 w_s}{\partial x \partial y}\right) - 2Y_{xx,xy} + Y_{yy,xy} - 1/2Y_{xy,yy} + 1/2Y_{xy,xx} = 0, \tag{16c}$$

$$\delta W_s = 0; -M_{x,x} - 2M_{xy,y} - M_{y,y} + N_{xx}\left(\frac{\partial^2 w_s}{\partial x^2} + \frac{\partial^2 w_b}{\partial x^2}\right) + N_{yy}\left(\frac{\partial^2 w_s}{\partial y^2} + \frac{\partial^2 w_b}{\partial y^2}\right) + 2N_{xy}\left(\frac{\partial^2 w_b}{\partial x \partial y} + \frac{\partial^2 w_s}{\partial x \partial y}\right) - Y_{xx,xy} + 1/2Y_{yy,xy} - 1/4Y_{xy,yy}, +1/4Y_{xy,xx} = 0 \tag{16d}$$

$$\delta \Phi = 0; \int_{-h/2}^{h/2}\left[\frac{\partial \widehat{D}_x}{\partial x}\cos(\beta z) + \frac{\partial \widehat{D}_y}{\partial y}\cos(\beta z) + \widehat{D}_z \beta \sin(\beta z)\right] dz = 0. \tag{16e}$$

N_i, M_i and Q_i $(i=x, y, xy)$ are the stress resultants and Y_{ij} $(i=x, y, xy)$ is the non-zero curvature resultant as follows:

$$(N_x, N_y, N_{xy}) = \int_{-h/2}^{h/2} (\sigma_x, \sigma_y, \sigma_{xy}) dz, \tag{17a}$$

$$(M_x, M_y, M_{xy}) = \int_{-h/2}^{h/2} (\sigma_x, \sigma_y, \sigma_{xy}) z dz, \tag{17b}$$

$$\left(Q_x, Q_y\right) = \int_{-h/2}^{h/2} (\sigma_{xz}, \sigma_{yz}) dz, \tag{17c}$$

$$\begin{Bmatrix} Y_{xx} \\ Y_{yy} \\ Y_{xy} \\ Y_{xz} \\ Y_{yz} \end{Bmatrix} = \int_{-h/2}^{h/2} \begin{Bmatrix} m_{xx} \\ m_{yy} \\ m_{xy} \\ m_{xz} \\ m_{yz} \end{Bmatrix} dz, \tag{18}$$

$$\begin{Bmatrix} \widehat{D}_x \\ \widehat{D}_y \\ \widehat{D}_z \end{Bmatrix} = \int_{-h/2}^{h/2} \begin{Bmatrix} D_x \cos(\beta z) \\ D_y \cos(\beta z) \\ D_z \beta \sin(\beta z) \end{Bmatrix} dz = \begin{Bmatrix} E_{15}\dfrac{\partial w_s}{\partial x} + X_{11}\dfrac{\partial \Phi}{\partial x} \\ E_{15}\dfrac{\partial w_s}{\partial y} + X_{11}\dfrac{\partial \Phi}{\partial y} \\ -E_{31}\dfrac{\partial^2 w_b}{\partial x^2} - E_{31}\dfrac{\partial^2 w_b}{\partial y^2} - X_{33}\Phi \end{Bmatrix}. \tag{19}$$

The coefficients in Eq. (19) can be expressed respectively.

$$\begin{Bmatrix} E_{31} \\ E_{15} \\ X_{11} \\ X_{33} \end{Bmatrix} = \int_{-h/2}^{h/2} \begin{Bmatrix} \widehat{e}_{31} \beta z \sin(\beta z) \\ \widehat{e}_{15} \beta \cos(\beta z) \\ \widehat{\kappa}_{11} \beta \cos^2(\beta z) \\ \widehat{\kappa}_{33} \beta^2 \sin^2(\beta z) \end{Bmatrix} dz. \tag{20}$$

Next, the governing equations (Eq. 16) for rectangular piezoelectric nanoplate can be rewritten:

$$N_{x,x} + N_{xy,y} + \frac{1}{2}A_s\left(-\frac{\partial^4 u}{\partial x^2 \partial y^2} + \frac{\partial^4 v}{\partial x^3 \partial y}\right) + \frac{1}{2}A_s\left(-\frac{\partial^4 u}{\partial y^4} + \frac{\partial^4 v}{\partial x \partial y^3}\right) = 0, \tag{21a}$$

$$N_{xy,x} + N_{y,y} - \frac{1}{2}A_s\left(-\frac{\partial^4 u}{\partial x^3 \partial y} + \frac{\partial^4 v}{\partial x^4}\right) - \frac{1}{2}A_s\left(-\frac{\partial^4 u}{\partial x \partial y^3} + \frac{\partial^4 v}{\partial x^2 \partial y^2}\right) = 0, \tag{21b}$$

$$Q_{x,x} + Q_{y,y} + N_{xx}\left(\frac{\partial^2 w_b}{\partial x^2} + \frac{\partial^2 w_s}{\partial x^2}\right) + N_{yy}\left(\frac{\partial^2 w_b}{\partial y^2} + \frac{\partial^2 w_s}{\partial y^2}\right) + 2N_{xy}\left(\frac{\partial^2 w_b}{\partial x \partial y} + \frac{\partial^2 w_s}{\partial x \partial y}\right) - \frac{5}{2}A_s\left(2\frac{\partial^4 w_b}{\partial x^2 \partial y^2} + \frac{\partial^4 w_s}{\partial x^2 \partial y^2}\right) - \frac{1}{4}A_s \times \left(2\frac{\partial^4 w_b}{\partial x^4} + \frac{\partial^4 w_s}{\partial x^4} + 2\frac{\partial^4 w_b}{\partial y^4} + \frac{\partial^4 w_s}{\partial y^4}\right) = 0, \tag{21c}$$

$$-M_{x,xx} - 2M_{xy,xy} - M_{y,yy} + N_{xx}\left(\frac{\partial^2 w_b}{\partial x^2} + \frac{\partial^2 w_s}{\partial x^2}\right) + N_{yy}\left(\frac{\partial^2 w_b}{\partial y^2} + \frac{\partial^2 w_s}{\partial y^2}\right) + 2N_{xy}\left(\frac{\partial^2 w_b}{\partial x \partial y} + \frac{\partial^2 w_s}{\partial x \partial y}\right) - \frac{1}{2}A_s\left(5\frac{\partial^4 w_b}{\partial x^2 \partial y^2} + 3\frac{\partial^4 w_s}{\partial x^2 \partial y^2}\right) - \frac{1}{4}A_s \times \left(\frac{\partial^4 w_b}{\partial x^4} + \frac{1}{2}\frac{\partial^4 w_s}{\partial x^4} + \frac{\partial^4 w_b}{\partial y^4} + \frac{1}{2}\frac{\partial^4 w_s}{\partial y^4}\right) = 0, \tag{21d}$$

$$\int_{-h/2}^{h/2}\left[\frac{\partial \widehat{D}_x}{\partial x}\cos(\beta z)+\frac{\partial \widehat{D}_y}{\partial y}\cos(\beta z)+\widehat{D}_z\beta\sin(\beta z)\right]dz=0. \tag{21e}$$

The axial and flexural rigidities of piezoelectric nanoplate are given by:

$$A_{ij}=\int_{-\frac{h}{2}}^{\frac{h}{2}}\widehat{C}_{ij}dz,\ D_{ij}=\int_{-\frac{h}{2}}^{\frac{h}{2}}\widehat{C}_{ij}z^2dz(i,j=1,2,6), \tag{22a}$$

$$\begin{cases}\widehat{C}_{11}=C_{11}-\dfrac{C_{13}^2}{C_{33}}\\ \widehat{C}_{12}=C_{12}-\dfrac{C_{13}^2}{C_{33}}\\ \widehat{C}_{44}=C_{44}\\ \widehat{C}_{66}=C_{66}\end{cases};\quad\begin{cases}\widehat{e}_{31}=e_{31}-\dfrac{C_{13}e_{33}}{C_{33}}\\ \widehat{e}_{15}=e_{15}\\ \widehat{\kappa}_{11}=\kappa_{11}\\ \widehat{\kappa}_{33}=\kappa_{33}+\dfrac{e_{33}^2}{C_{33}}\end{cases}. \tag{22b}$$

In Eq. (22), A_{ij} and D_{ij} are extensional stiffness and extension-bending coupling matrix, respectively. The stress resultants in Eq. (17) in displacement field by using Eq. (22) and substituting in Eq. (17) are defined as:

$$\begin{bmatrix}N_{xx}\\N_{yy}\\N_{xy}\\M_{xx}\\M_{yy}\\M_{xy}\\Q_y\\Q_x\end{bmatrix}=\begin{bmatrix}A_{11}&A_{12}&0&0&0&0&0&0\\A_{21}&A_{22}&0&0&0&0&0&0\\0&0&A_{66}&0&0&0&0&0\\0&0&0&D_{11}&D_{12}&0&0&0\\0&0&0&D_{21}&D_{22}&0&0&0\\0&0&0&0&0&D_{66}&0&0\\0&0&0&0&0&0&A_{44}&0\\0&0&0&0&0&0&0&A_{44}\end{bmatrix}\times\begin{bmatrix}\dfrac{\partial u}{\partial x}+\dfrac{1}{2}\left(\dfrac{\partial w_b}{\partial x}\right)^2+\dfrac{1}{2}\left(\dfrac{\partial w_s}{\partial x}\right)^2+\dfrac{\partial w_b}{\partial x}\dfrac{\partial w_s}{\partial x}\\ \dfrac{\partial v}{\partial y}+\dfrac{1}{2}\left(\dfrac{\partial w_b}{\partial y}\right)^2+\dfrac{1}{2}\left(\dfrac{\partial w_s}{\partial y}\right)^2+\dfrac{\partial w_b}{\partial y}\dfrac{\partial w_s}{\partial y}\\ \dfrac{\partial u}{\partial y}+\dfrac{\partial v}{\partial x}+\left(\dfrac{\partial w_b}{\partial x}+\dfrac{\partial w_s}{\partial x}\right)\left(\dfrac{\partial w_b}{\partial y}+\dfrac{\partial w_s}{\partial y}\right)\\ -\dfrac{\partial^2 w_b}{\partial x^2}\\ -\dfrac{\partial^2 w_b}{\partial y^2}\\ -\dfrac{\partial^2 w_b}{\partial x\partial y}\\ \dfrac{\partial w_s}{\partial y}\\ \dfrac{\partial w_s}{\partial x}\end{bmatrix}+\begin{Bmatrix}2\widehat{e}_{31}V_0\\2\widehat{e}_{31}V_0\\0\\E_{31}\Phi\\E_{31}\Phi\\0\\-E_{15}\dfrac{\partial\Phi}{\partial y}\\-E_{15}\dfrac{\partial\Phi}{\partial x}\end{Bmatrix}. \tag{23}$$

The in-plane shear force in pre-buckling conditions is as follows [22]:

$$N_{xy}=-N^0 \tag{24}$$

N^0 is critical shear in-plane load in buckling conditions. Inserting Eqs. (18, 19) and (23) into Eqs. (21), and also by considering the pre-buckling conditions the electro-mechanical stability equations in the form of displacement components based on S-FSDT also including couple stress effect are expressed as follows:

$$\begin{aligned}&H_{44}\frac{\partial^2 w_s}{\partial x^2}+H_{55}\frac{\partial^2 w_s}{\partial y^2}-2N^0\left(\frac{\partial^2 w_b}{\partial x\partial y}+\frac{\partial^2 w_s}{\partial x\partial y}\right)+2\widehat{e}_{31}V_0\left(\frac{\partial^2 w_b}{\partial x^2}+\frac{\partial^2 w_s}{\partial x^2}\right)+2\widehat{e}_{31}V_0\left(\frac{\partial^2 w_b}{\partial y^2}+\frac{\partial^2 w_s}{\partial y^2}\right)\\&-E_{15}\frac{\partial^2\Phi}{\partial x^2}-E_{15}\frac{\partial^2\Phi}{\partial y^2}-A_s\left[\frac{5}{2}\left(2\frac{\partial^4 w_b}{\partial x^2\partial y^2}+\frac{\partial^4 w_s}{\partial x^2\partial y^2}\right)-\frac{1}{4}\left(2\frac{\partial^4 w_b}{\partial x^4}+\frac{\partial^4 w_s}{\partial x^4}+2\frac{\partial^4 w_b}{\partial y^4}+\frac{\partial^4 w_s}{\partial y^4}\right)\right]=0\\&D_{11}\frac{\partial^4 w_b}{\partial x^4}+(2D_{12}+2D_{66})\frac{\partial^4 w_b}{\partial x^2\partial y^2}+D_{22}\frac{\partial^4 w_b}{\partial y^4}-2N^0\left(\frac{\partial^2 w_b}{\partial x\partial y}+\frac{\partial^2 w_s}{\partial x\partial y}\right)+2\widehat{e}_{31}V_0\left(\frac{\partial^2 w_b}{\partial x^2}+\frac{\partial^2 w_s}{\partial x^2}\right)\\&+2\widehat{e}_{31}V_0\left(\frac{\partial^2 w_b}{\partial y^2}+\frac{\partial^2 w_s}{\partial y^2}\right)+E_{31}\frac{\partial^2\Phi}{\partial x^2}+E_{31}\frac{\partial^2\Phi}{\partial y^2}-A_s\left[\frac{1}{2}\left(5\frac{\partial^4 w_b}{\partial x^2\partial y^2}+3\frac{\partial^4 w_s}{\partial x^2\partial y^2}\right)\right.\\&\left.-\frac{1}{4}\left(\frac{\partial^4 w_b}{\partial x^4}+\frac{1}{2}\frac{\partial^4 w_s}{\partial x^4}+\frac{\partial^4 w_b}{\partial y^4}+\frac{1}{2}\frac{\partial^4 w_s}{\partial y^4}\right)\right]=0\\&E_{15}\left(\frac{\partial^2 w_s}{\partial x^2}+\frac{\partial^2 w_s}{\partial y^2}\right)-E_{31}\left(\frac{\partial^2 w_b}{\partial x^2}+\frac{\partial^2 w_b}{\partial y^2}\right)+X_{11}\left(\frac{\partial^2\Phi}{\partial x^2}+\frac{\partial^2\Phi}{\partial y^2}\right)-X_{33}\Phi=0.\end{aligned} \tag{25a-c}$$

3. Analytical solution

In the paper, different analytical boundary conditions are applied to solve the obtained stability equations which can be written in an explicit mathematically form as [21,35–36]

$$\text{Free edges}(F):X_i=\left[\sin^2(\alpha_i x_i)+1\right]\cos^2(\alpha_i x_i);\ i=1,2, \tag{26a}$$

Table 1
Comparison of results for critical biaxial buckling load for single-layered graphene sheet and all edges simply supported obtained from DQ method [19,37], and molecular dynamics simulation [38].

Critical buckling load (Pa m)				
S-FSDT, Exact present study	FSDT-DQM [19]	FSDT-DQM [37]	MD results [38]	$Lx = Ly$ (nm)
1.0835	1.0749	1.0809	1.0837	4.99
0.6538	0.6523	0.6519	0.6536	8.080
0.4330	0.4356	0.4350	0.4331	10.77
0.2615	0.2645	0.2639	0.2609	14.65
0.1720	0.1751	0.1748	0.1714	18.51
0.1198	0.1239	0.1237	0.1191	22.35
0.0896	0.0917	0.0914	0.0889	26.22
0.0696	0.0707	0.0705	0.0691	30.04
0.0559	0.0561	0.0560	0.0554	33.85
0.0454	0.0453	0.0451	0.0449	37.81

$$\text{Clamped } (\mathbf{C}): X_i = \sin^2(\alpha_i x_i);\ \mathrm{i} = 1, 2, \tag{26b}$$

$$\text{Simply supported}(\mathrm{S}): X_i = \sin(\alpha_i x_i);\ \mathrm{i} = 1, 2, \tag{26c}$$

in which m and n are the half wave numbers, $\alpha_1 = m\pi/Lx$, $\alpha_2 = n\pi/Ly$; $x_1 = x$, $x_2 =$ y or terms used in the x and y direction to represent the displacement functions. We use the displacement function in the following form:

$$w_k(x, y) = \sum_{m,n=1}^{\infty} W_k \times X_i \times X_j;\ k = s, b;\ i = 1, 2;\ j = 1, 2 \tag{27a}$$

$$\Phi(x, y) = \sum_{m,n=1}^{\infty} \Phi \times X_i \times X_j;\ i = 1, 2;\ j = 1, 2. \tag{27b}$$

Substituting the expression of w_k,Φ in Eqs. (27a,b) can obtain the explicit relation for buckling loads with various boundary conditions. The stability equations and closed-form boundary conditions yield a set of following algebraic equations:

$$\begin{Bmatrix} \text{Eq. (25a)} \\ \text{Eq. (25b)} \\ \text{Eq. (25c)} \end{Bmatrix} = \begin{bmatrix} k_{11} & k_{12} & k_{13} \\ k_{21} & k_{22} & k_{23} \\ k_{31} & k_{32} & k_{33} \end{bmatrix} \begin{Bmatrix} W_b \\ W_s \\ \Phi \end{Bmatrix}. \tag{28}$$

k_{ij} ($i, j = 1, 2$) are the coefficients of constants terms through which to obtain the critical force are as follows:

$$q = \begin{bmatrix} Eq.(25a) & Eq.(25b) & Eq.(25c) \end{bmatrix}, u = \begin{bmatrix} W_b & W_s & \Phi \end{bmatrix}, \tag{29}$$

$$J = jacobian(q, u) \rightarrow \det[J] = 0. \tag{30}$$

The critical shear buckling load (N^0) can be easily obtained by solving Eq. (30).

4. Results and discussions

The results validation and comparison with other research results should obviously be carried out before investigating various parameters of this article. Because of this fact that there are not any available papers in the field of shear buckling of piezoelectric nanoplates, therefore, Tables 1 and 2 which were in nanoplates field are examined in order to compare and validate this formulation results with those of other articles. In order for the results to be compared in Tables 1 and 2, [19] and [37] were employed while their results are obtained using first order shear deformation theory, differential quadrature method (DQM), as well as Eringen nonlocal elasticity theory. Ref. [38] is added for further confirmation due to the minor errors in the numerical solutions, and its results are obtained through molecular dynamics solution. Therefore, observing numerical solution alone does not enable us to ascertain the fact that the present results are validated due to the difference between the results in both cases. However, by examining Tables 1 and 2, one can strongly express that the modified first order shear deformation theory (S-FSDT) results appropriately correspond to the molecular dynamic results. Since this solution is an exact one, this proximity of the results clearly confirms this premise that accurate and appropriate results are obtained by combining the modified first order shear deformation theory and exact solution of the results. Comparing the results shown in Tables 1 with 2 confirms that the removal of the shear stress correction factors in plates affects the critical load results. Because, the difference generated in the contractual FSDT by employing this factor when compared with the accurate results, is removed in the S-FSDT. According to Tables 1, and 2 the thinner we assume the plate, the closer the

Table 2
Comparison of the present results with those of DQ method [37] and molecular dynamics (MD) simulation [38] for different aspect ratios of orthotropic single-layered graphene sheets under uniform biaxial compression.

Critical buckling load (*Pa.m*)			
FSDT-DQM [37]	MD results [38]	S-FSDT, Exact present study	*Lx*/*Ly*
0.5115	0.5101	0.5105	0.5
0.5715	0.5693	0.5698	0.75
0.6622	0.6595	0.6599	1.25
0.7773	0.7741	0.7747	1.5
1.0222	1.0183	1.0180	1.75
1.1349	1.1297	1.1301	2

Table 3
Mechanical and electrical properties of piezoelectric nanoplate.

Piezoelectric nanoplate	$C_{11}=132$ GPa, $C_{12}=71$ GPa, $C_{13}=73$ GPa, $C_{33}=115$ GPa, $C_{44}=26$ GPa, $C_{66}=30.5$ GPa, $h=0.34$ nm, $e_{31}=-4.1$ C/m^2, $e_{15}=10.5$ C/m^2, $e_{33}=14.1$ C/m^2 (Coulombs = C = Nm/V), $\kappa_{11}=5.841e{-}9$ C/Vm, $\kappa_{33}=7.124e{-}9$ C/V m

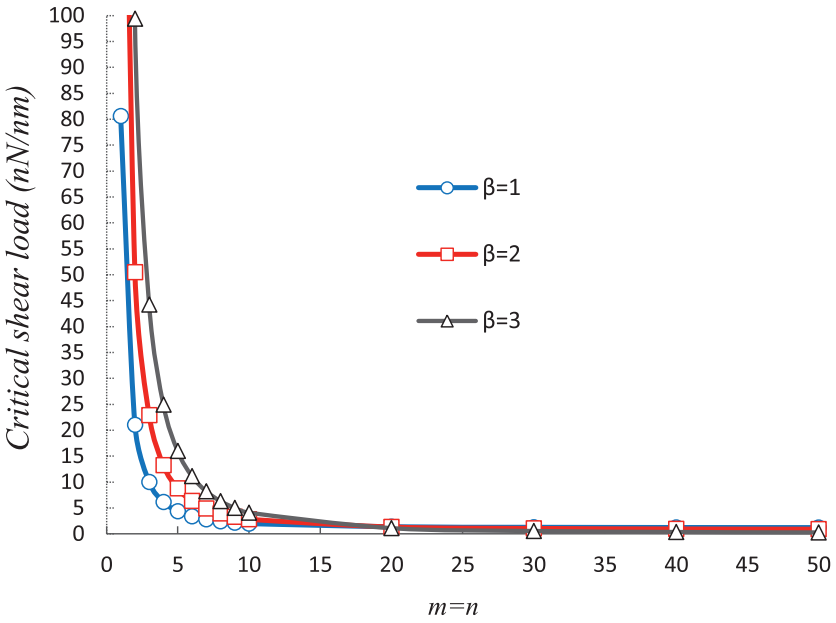

Fig. 2. The effect of β parameter versus wave numbers ($\beta = Lx/Ly$, $Ly = 30$ h, $l = h$, $V_0 = 0.05$ V, SSSS).

results become to the FSDT results and numerical solution, while their accuracy decreases; because, FSDT is not applicable to analyze thin plates and the classical plate theory (CPT) is more applicable in this case.

$E = 1$ TPa, $\upsilon = 0.3$, $h = 0.34$ nm, $\mu = 1.81$ nm^2, $\beta = Lx/Ly = 1$, $k1 = 1$, $k2 = 1$, $k_s = 5/6$, SSSS [19,37,38]
$E = 1$ TPa, $\upsilon = 0.3$, $h = 0.34$ nm, $\beta = 1$, $k1 = 1$, $k2 = 1$, $l = .91$ nm, $\eta = 0$, SSSS [Present]

In order to solve stability equations, the parameters in Table 3 obtained from credible related research [32] are employed. Fig. 2 shows m and n variations for square and rectangular nano-piezoelectric-sheets. It is clear that results are not accurate before $m = n = 20$, but after $m = n > 20$ the critical shear loads almost converge to the point that m and n variations have no effect on critical shear load at $m = n > 30$. Therefore, the results at $m = n = 30$ are convenient for extracting the critical shear load of piezoelectric nano-sheets from.

Fig. 3 shows the variations of length scale versus length to thickness ratio of the sheet. It is seen that critical shear load increases with length scale. Results were extracted for clamped boundary conditions with the external voltage being 0.05 V. According to the Figure, the critical shear load decreases as the sheet length to thickness ratio increases. The Figure is plotted for a thin sheet $Lx/h \geq 30$ and a medium thickness sheet $10 \geq Lx/h \geq 20$. In fact, as the sheet becomes thinner, the critical load decreases which is a logical outcome.

In order to study the effect of length scale on different boundary conditions, Fig. 4 was examined. It was found that with a more flexible boundary condition critical load results decrease, which means that the maximum critical shear load occurs

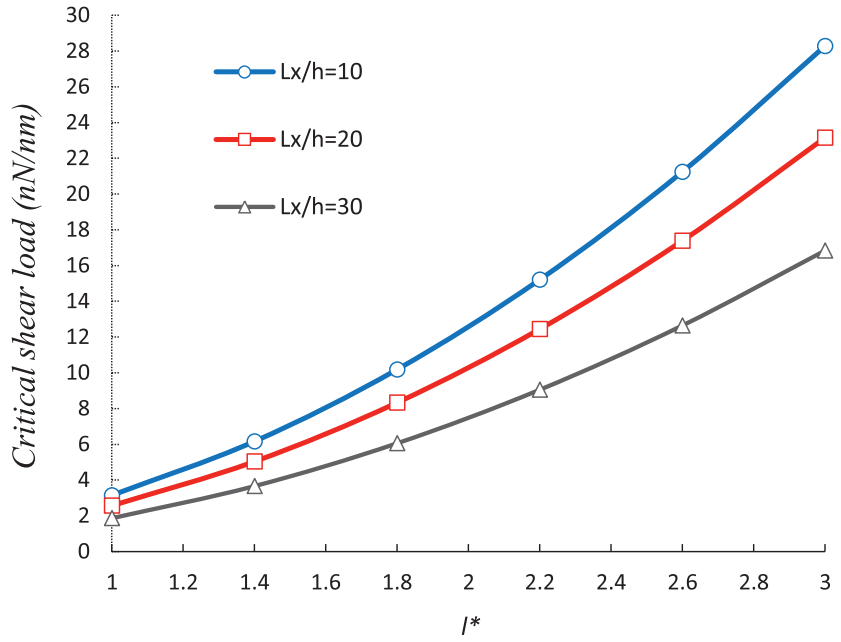

Fig. 3. Length scale parameter versus length to thickness ratio ($Ly = 30\,h$, $l^* = l/h$, $V_0 = 0.05$ V, CCCC).

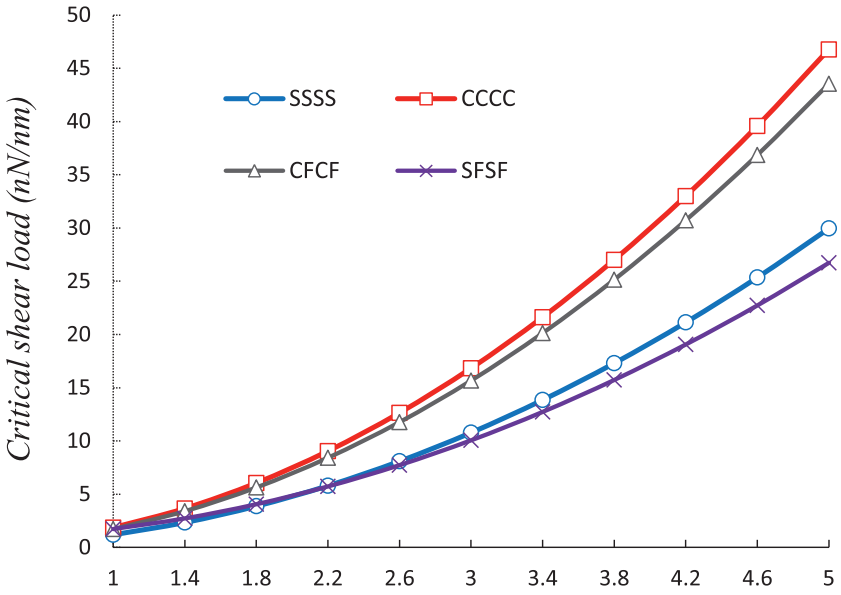

Fig. 4. The length scale parameter versus boundary conditions ($Lx = Ly = 30\,h$, $l^* = l/h$, $V_0 = 0.05$ V).

with clamped boundary conditions providing the minimum flexibility. The critical shear load at $l^* > 1.8$ is greater for SFSF condition than for SSSS. The reason is different length scales in different boundary conditions.

Fig. 5a and b is plotted to examine the effect of external electric voltage applied to the piezoelectric nano-sheet versus the length to thickness ratio and β parameter. Fig. 5a is extracted for clamped boundary conditions while Fig. 5b pertains to simply supported boundary conditions. Fig. 5a suggests that with clamped boundary conditions, critical shear load increases with external voltage, but the effect of external voltage on critical load is negligible. Fig. 5b presents dissimilar results, since for simply supported boundary conditions, the critical shear load decreases with increasing external voltage. Furthermore, it is evident that with an increased length to width ratio the shear load decreases and external voltage becomes more effective. The difference in results of the diagrams proves the statement.

Fig. 6 shows the direct effect of external voltage on critical shear load. Results were extracted for CFCF boundary conditions and suggest that the effect of external voltage on critical shear load is negligible. Table 4 is presented to verify this

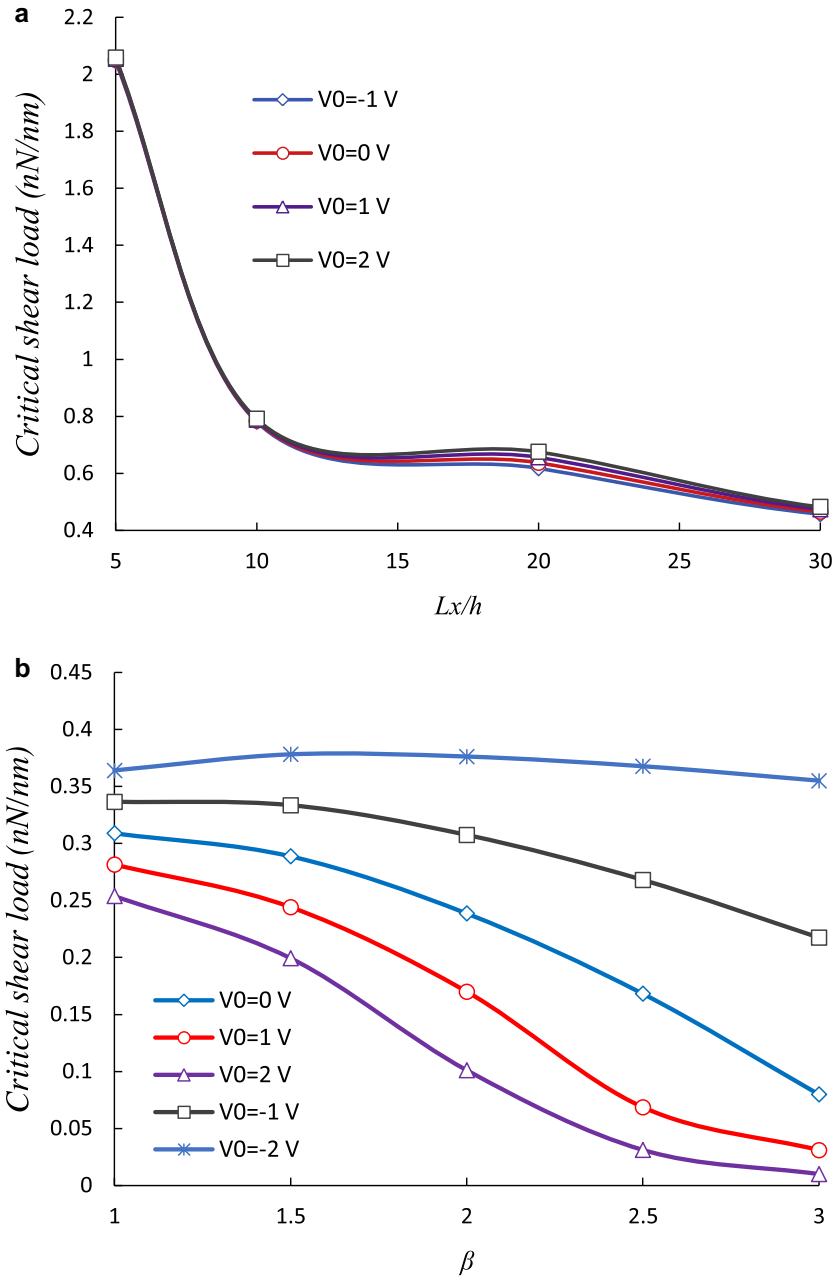

Fig. 5. (a) The effect of external voltage versus length to thickness ratio ($Ly = 30\,h$, $l = 0.5\,h$, CCCC). (b) The effect of various external voltage versus β parameter ($Ly = 30\,h$, $l = 0.5\,h$, SSSS).

fact. It is clear that the critical shear load increases with external voltage in CCCC boundary conditions while it decreases with the other two boundary conditions. Moreover, with the external voltage increased, minute differences appear in critical shear load results, showing the effect of external voltage on critical shear load to be negligible. In fact, the shear load occurring on the piezoelectric nano-sheet due to external electric current is insignificant.

5. Conclusions

This study investigated the shear buckling of piezoelectric nanoplate under external electric voltage. In this regard, modified first order shear deformation theory was employed to obtain the governing equations by taking Von-Karman nonlinear strains into consideration. The impact of small scale was investigated by using modified couple stress theory. Moreover, the

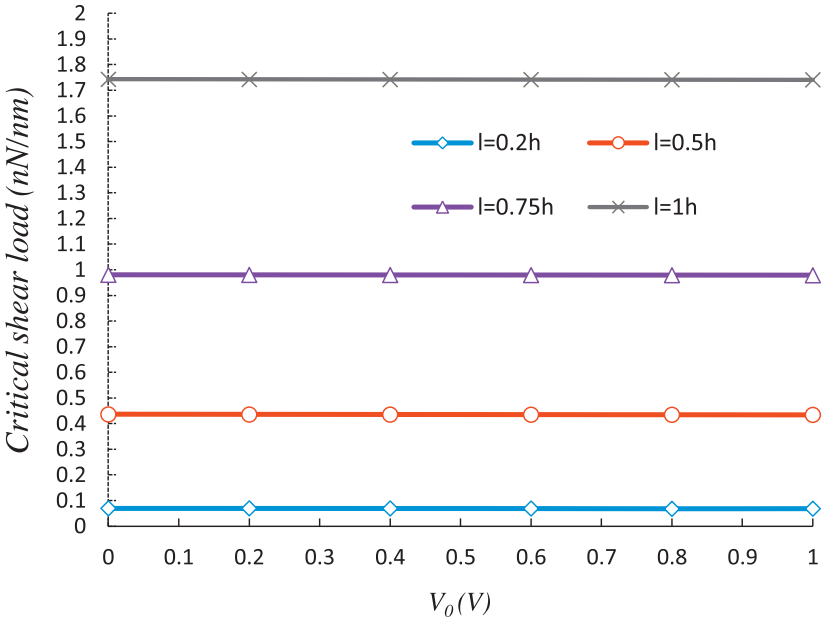

Fig. 6. The effect of various length scale parameter versus external voltage ($Ly = 30\,h$, CFCF).

Table 4
The effect of external electric voltage on various boundary conditions.

(Ly = 30 h, l = h) Critical shear buckling load (nN/nm)			
V_0 *(V)*	CCCC	CFCF	SSSS
−1.5	1.8554	1.7455	1.2494
−1	1.8597	1.7446	1.2356
−0.5	1.8640	1.7437	1.2218
0	1.8682	1.7428	1.2081
0.5	1.8725	1.7419	1.1943
1	1.8768	1.7410	1.1806
1.5	1.8811	1.7401	1.1668
2	1.8853	1.7392	1.1531
2.5	1.8896	1.7384	1.1393
3	1.8939	1.7375	1.1255
3.5	1.8982	1.7366	1.1118
4	1.9024	1.7357	1.0980
4.5	1.9067	1.7348	1.0843
5	1.9110	1.7339	1.0705

exact solution was used to extract the results by changing various parameters. In conclusion, some of the important results achieved from the present study are as follows:

- By increasing the parameter β, the impact of external electric voltage on the results of the critical shear load increases.
- Exact solutions by S-FSDT theory are satisfactorily corresponding to the molecular dynamics solution.
- Whenever the boundary conditions are less flexible, the critical shear load will increase.
- The length scale impact on the results of any boundary conditions increases with an increase in l parameters.
- By increasing the external electric voltage, the critical shear load in flexible boundary conditions decreases and vice versa in non-flexible boundary conditions.
- The effect of external electric voltage on the critical shear load occurring on the piezoelectric nanoplate is insignificant.

References

[1] Z. Zhang, Size-Dependent Electroelastic Properties of Piezoelectric Nanoplates, Electronic Thesis and Dissertation Repository. Paper 2207, 2014.
[2] S. Mishra, B.K. Sethy, Nano-Indentation of Copper-Nickel Thin Films—A Molecular Dynamics Simulation Study, National Institute of Technology, Rourkela, 2013.
[3] C.L. Sun, J. Shi, X.D. Wang, Fundamental study of mechanical energy harvesting using piezoelectric nanostructures, J. Appl. Phys. 108 (2010) 034309.
[4] L.C. Lew, Y. Voon, M. Willatzen, Electromechanical phenomena in semiconductor nanostructures, J. Appl. Phys. 109 (2011) 031101.

[5] X.Q. Fang, J.X. Liu, V. Gupta, Fundamental formulations and recent achievements in piezoelectric nano-structures: a review, Nanoscale 5 (2013) 1716–1726.
[6] Ö. Civalek, Ç. Demir, B. Akgöz, Free Vibration and bending analysis of cantilever microtubules based on nonlocal continuum model, Math. Comput. Appl. 15 (2010) 289–298.
[7] B. Akgöz, Ö. Civalek, Strain gradient elasticity and modified couple stress models for buckling analysis of axially loaded micro-scaled beams, Int. J. Eng. Sci. 49 (2011) 1268–1280.
[8] P. Malekzadeh, A.R. Setoodeh, A.A. Beni, Small scale effect on the thermal buckling of orthotropic arbitrary straight-sided quadrilateral nanoplates embedded in an elastic medium, Compos. Struct. 93 (2011) 2083–2089.
[9] L.L. Ke, Y.S. Wang, Z.D. Wang, Nonlinear vibration of the piezoelectric nanobeams based on the nonlocal theory, Compos. Struct 94 (2012) 2038–2047.
[10] C. Liu, L.L. Ke, Y.S. Wang, J. Yang, S. Kitipornchai, Buckling and post-buckling of size-dependent piezoelectric Timoshenko nanobeams subject to thermo-electro-mechanical loadings, Int. J. Struct. Stab. Dyn. 14 (2014) 1350067.
[11] T. Murmu, J. Sienz, S. Adhikari, C. Arnold, Nonlocal buckling of double-nanoplate-systems under biaxial compression, Compos. Part B 44 (2013) 84–94.
[12] P. Malekzadeh, A. Alibeygi, Thermal buckling analysis of orthotropic nanoplates on nonlinear elastic foundation, Encyclopedia of Thermal Stresses, 2014, pp. 4862–4872.
[13] M. Mohammadi, A. Farajpour, A. Moradi, M. Ghayour, Shear buckling of orthotropic rectangular graphene sheet embedded in an elastic medium in thermal environment, Compos.: Part B 56 (2014) 629–637.
[14] N. Radic, D. Jeremic, S. Trifkovic, M. Milutinovic, Buckling analysis of double-orthotropic nanoplates embedded in Pasternak elastic medium using nonlocal elasticity theory, Compos.: Part B 61 (2014) 162–171.
[15] D. Karlicic, S. Adhikari, T. Murmu, Exact closed-form solution for non-local vibration and biaxial buckling of bonded multi-nanoplate system, Compos.: Part B 66 (2014) 328–339.
[16] A. Anjomshoa, A.R. Shahidi, B. Hassani, E. Jomehzadeh, Finite Element buckling analysis of multi-layered graphene sheets on elastic substrate based on nonlocal elasticity theory, App. Math. Model. 38 (2014) 1–22.
[17] I.S. Radebe, S. Adali, Buckling and sensitivity analysis of nonlocal orthotropic nanoplates with uncertain material properties, Compos.: Part B 56 (2014) 840–846.
[18] L.Y. Jiang, Z. Yan, Vibration and buckling analysis of a piezoelectric nanoplate considering surface effects and in-plane constraints, Proc. R. Soc. A. 468 (2012) 3458–3475.
[19] M.E. Golmakani, J. Rezatalab, Nonuniform biaxial buckling of orthotropic Nano plates embedded in an elastic medium based on nonlocal Mindlin plate theory, Compos. Struct. 119 (2015) 238–250.
[20] N. Challamel, F. Hache, I. Elishakoff, C.M. Wang, Buckling and vibrations of micro structured rectangular plates considering phenomenological and lattice-based nonlocal continuum models, Compos. Struct. 149 (2016) 145–156.
[21] N. Radic, D. Jeremić, Thermal buckling of double-layered graphene sheets embedded in an elastic medium with various boundary conditions using a nonlocal new first-order shear deformation theory, Compos.: Part B 97 (2016) 201–215.
[22] M. Malikan, M. Jabbarzadeh, Sh. Dastjerdi, Non-linear Static stability of bi-layer carbon nanosheets resting on an elastic matrix under various types of in-plane shearing loads in thermo-elasticity using nonlocal continuum, Microsyst. Technol (2016), doi:10.1007/s00542-016-3079-9.
[23] R.D. Mindlin, Influence of rotatory inertia and shear on flexural motions of isotropic, elastic plates, Trans. ASME 73 (1951) 31–38.
[24] H.T. Thai, D.H. Choi, A simple first-order shear deformation theory for laminated composite plates, Compos. Struct. 106 (2013) 754–763.
[25] R.D. Mindlin, H.F. Tiersten, Effects of couple-stresses in linear elasticity, Arch. Ration. Mech. Anal 11 (1962) 415–448.
[26] R.A. Toupin, Elastic materials with couple stresses, Arch. Ration. Mech. Anal. 11 (1962) 385–414.
[27] W.T. Koiter, Couple stresses in the theory of elasticity, I and II, Proc K Ned Akad Wet (B) 67 (1964) 17–44.
[28] E. Cosserat, F. Cosserat, Theory of deformable bodies, in: D.H. Delphenich (Ed.), Scientific Library, 6, 6, A. Herman and Sons, Sorbonne, Paris, 1909.
[29] F. Yang, A.C.M. Chong, D.C.C. Lam, P. Tong, Couple stress based strain gradient theory for elasticity, Int. J Solids Struct. 39 (2002) 2731–2743.
[30] B. Akgöz, Ö. Civalek, Free vibration analysis for single-layered graphene sheets in an elastic matrix via modified couple stress theory, Mater. Des 42 (2012) 164–171.
[31] H.T. Thai, P.V. Thuc, T.K. Nguyen, J. Lee, Size-dependent behavior of functionally graded sandwich microbeams based on the modified couple stress theory, Compos. Struct. 123 (2015) 337–349.
[32] C. Liu, L.L. Ke, J. Yang, S. Kitipornchai, Y.S. Wang, Buckling and post-buckling analysis of size-dependent piezoelectric nanoplates, Theor. Appl. Mech. Lett (2016). http://dx.doi.org/10.1016/j.taml.2016.10.003.
[33] L.L. Ke, C. Liu, Y.S. Wang, Free vibration of nonlocal piezoelectric nanoplates under various boundary conditions, Phys. E 66 (2015) 93–106.
[34] Q. Wang, Axi-symmetric wave propagation in a cylinder coated with a piezoelectric layer, Int. J. Solid Struct. 39 (2002) 3023–3037.
[35] HT. Thai, TK. Nguyen, TP. Vo, J. Lee, Analysis of functionally graded sandwich plates using a new first-order shear deformation theory, Eur. J. Mech.-A/Solids 45 (2014) 211–225.
[36] M. Sobhy, Buckling and free vibration of exponentially graded sandwich plates resting on elastic foundation under various boundary conditions, Compos. Struct. 99 (2013) 76–87.
[37] M.E. Golmakani, M.N. Sadraee Far, Buckling analysis of biaxially compressed double-layered graphene sheets with various boundary conditions based on nonlocal elasticity theory, Microsyst. Technol. (2016), doi:10.1007/s00542-016-3053-6.
[38] R. Ansari, S. Sahmani, Prediction of biaxial buckling behavior of single-layered graphene sheets based on nonlocal plate models and molecular dynamics simulations, Appl. Math. Model. 37 (2013) 7338–7351.